Asian Journal of Chemistry; Vol. 37, No. 11 (2025), 2753-2758
ASIAN JOURNAL OF CHEMISTRY
https://doi.org/10.14233/ajchem.2025.34566

Development of Samarium and Cerium Doped Yttrium Orthoborate Phosphor for near UV LED Application

R.M. VIMALATHITHAN[1], R. SATHEESH KUMAR[2,*], G. SURESH[3], D. BALAJI[4], S. BALASARASWATHY[5] and V. PONNUSAMY[6]

[1]Department of Physics, Salem Sowdeswari College (Government Aided), Salem-636010, India
[2]Department of Physics, C.K. College of Engineering and Technology, Cuddalore-608003, India
[3]Department of Humanities and Sciences/Physics Division, Centre for Nanotechnology Research, Aarupadai Veedu Institute of Technology, Vinayaka Mission's Research Foundation (D.U), Chennai-603104, India
[4]Centre for Nanoscience and Nanotechnology Sathyabama Institute of Science and Technology, Chennai-600119, India
[5]Department of Physics, BNM Institute of Technology, Bangalore-560070, India
[6]Solid-State Luminescence Lab, Department of Applied Sciences and Humanities, MIT Campus, Anna University, Chennai-600044, India

*Corresponding author: E-mail: satheshagas@gmail.com

Received: 30 July 2025 *Accepted*: 21 September 2025 *Published online*: 27 October 2025 AJC-22163

Inorganic phosphors are integral to light-emitting diode (LED) technology, enabling the generation of specific colours and white light for a variety of applications. In this study, yttrium orthoborate (YBO_3), a chemically stable and thermally robust host lattice, was successfully synthesized *via* a conventional solid-state reaction method. The synthesized material was systematically characterized using powder X-ray diffraction (XRD) to confirm phase purity and crystalline structure. Photoluminescence (PL) spectroscopy was employed to evaluate the photoluminescence properties of the phosphor. The results suggest that YBO_3 is a promising host matrix for rare-earth doping in phosphor-converted LED systems. Lanthanide ions such as samarium (Sm^{3+}) and cerium (Ce^{3+}) were incorporated into the YBO_3 host lattice to investigate their influence on the PL properties. PL measurements revealed that the doped phosphors exhibit strong excitation in the near-ultraviolet (UV) region. The resulting emission bands were observed within the visible spectrum. The optimal doping concentrations of Sm^{3+} and Ce^{3+} were determined based on the maximum emission intensity. These findings suggest that Sm^{3+}- and Ce^{3+}-doped YBO_3 phosphors are promising candidates for near-UV excited white LED applications.

Keywords: Yttrium borate, Orthorhombic phase with *Cmcm* space group, Samarium, Cerium.

INTRODUCTION

Luminescence materials (phosphors) have prospective applications in various fields including solid state lighting (SSL), displays, radiation dosimetry, security inks, horticulture and thermometry [1-4]. Phosphors produce the white light in SSL by appropriate colour combinations. A variety of optical materials based on oxides, borates, silicates, aluminates and sulfides were utilized as host matrix for SSL application [5]. Among them, borate compounds received substantial attention in the field of optical materials research due to their wide-ranging crystal structures, broad UV-Vis transmittance and large band gap (> 3 eV). Moreover, borates acquired high chemical and physical stability at high temperatures. These special properties made the borate as unique host matrix to find applications in various devices/modules [1-4]. By all of borates, vaterite-type yttrium orthoborate (YBO_3) doped with rare earth ions showed excellent optical properties for fascinating applications in these devices/modules.

The YBO_3 host itself does not possess any luminescent characteristics or properties. To induce luminescence property in YBO_3, transition or rare earth (lanthanides) metal ions must be used as dopants. Since, YBO_3 provides a wide variety of luminescence emission centres for dopants, as it crystallizes in different crystal structures [6,7]. Hence, the synthesis and study of the luminescence properties of YBO_3 has been considered an important one. Some of the quoted applications of rare earths doped YBO_3 are plasma display panels, phosphor

converted light emitting diodes, fluorescent lamps and security inks [8-14]. There are several well-known methods to synthesize phosphors, including solid-state reaction, combustion synthesis, sol-gel processing, co-precipitation and hydrothermal techniques [15]. Among these, the solid-state reaction method stands out for its straightforward approach and practicality, especially for producing yttrium borate on a larger scale. Unlike other techniques that often require multiple steps such as purification, filtration, removal of residual byproducts and precise control of reaction conditions, the solid-state route simplifies these complexities considerably.

In this work, we prepared both pure and doped yttrium borate phosphors by following the solid-state reaction method and examined their photoluminescent properties. Samarium (Sm^{3+}) and cerium (Ce^{3+}) ions were chosen as dopants due to their distinctive emission characteristics. Samarium typically emits in the red-orange region, while cerium can emit from blue-violet to yellow, depending on the host matrix environment. Doping YBO_3 with Sm^{3+} and Ce^{3+} is expected to generate visible emissions spanning multiple colours, which could be particularly beneficial for applications in solid-state lighting (SSL).

EXPERIMENTAL

Synthesis of YBO_3: To synthesize YBO_3, the solid-state reaction method was employed. Analytically pure A.R. grade precursors were used, so no need for further purification. The exact stochiometric ratio of precursors such as Y_2O_3 and H_3BO_3 was weighed. The weighed precursor salts were ground in an agate mortar for with ultimate mixing. The ground samples were pre-fired at 500 ºC for 2 h in a muffle furnace. The pre-fired sample was often ground well for 0.5 h using an agate mortar and subsequently annealed at 1000 ºC, 2 h. The entire process was carried out in an air atmosphere. Finally, pure white coloured powder samples were obtained. For dopants, Sm_2O_3 and Ce_2O_4 were used.

Characterization: X-ray diffraction (XRD) patterns of the synthesized YBO_3 sample were recorded between the 2θ values 10-80º with a step of 0.02º per 0.5 second at room temperature. Spectrum recorded using a BRUKER XRD instrument model D2 PHASER with Cu*K*α radiation (1.5405 Å). The photoluminescence (PL) measurements of YBO_3 phosphors were carried out using JOBIN YVON-Spex spectrofluorometer (Fluorolog version-3; model FL3-11) with a 150W Xenon lamp.

RESULTS AND DISCUSSION

XRD studies: The synthesized YBO_3 sample was subjected to powder X-ray diffraction analysis for crystal phase identification. The powder XRD pattern of the synthesized yttrium borate sample is shown in Fig. 1. The diffraction peaks found in the diffractogram are compared with standard JCPDS files of yttrium orthoborate. All the diffraction peaks (20.44º, 27.52º, 29.37º, 34º, 41.21º, 48.36º, 50.12º, 52.98º, 56.40º, 57.40º, 60.51º, 63.54º, 65.28º, 70.43º, 72.00º and 77.27º) are coincides with the standard JCPDS file No: 89-3501. Structural analysis revealed that the sample crystallizes in

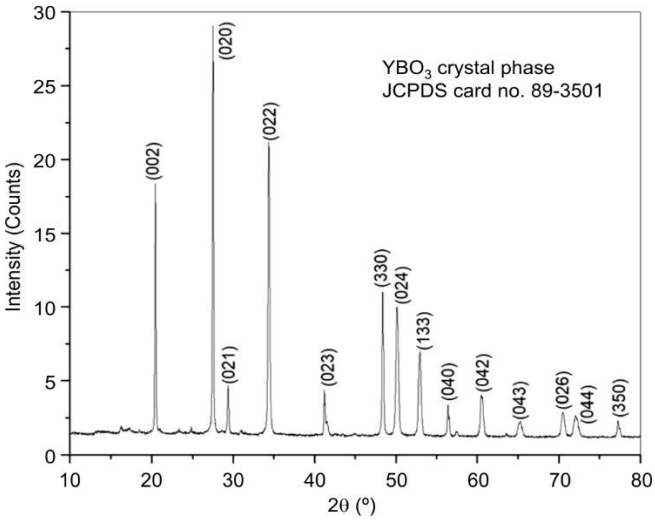

Fig. 1. X-ray diffraction pattern of YBO_3 sample

the orthorhombic *Cmcm* space group (No. 63), which is one of the characteristic space groups associated with specific phases of YBO_3. The presence of sharp and intense peaks in the XRD pattern indicates that the synthesized samples exhibit high crystallinity and belong to a centrosymmetric molecular structure. To gain deeper insight into the structural details, Rietveld refinement was performed on the XRD data. The refinement results are illustrated in Fig. 2, where the observed data points (crosses), calculated pattern (red line) and the difference between them (blue line) are shown. The close agreement between the observed and calculated profiles confirms the reliability of the structural model and the quality of the synthesized phase. Moreover, the reliability factors of the executed refinement were found to be R_{wp} = 5.55%, R_p = 9.83% and χ^2 = 2.13. Calculated lattice parameters are a = 11.351(2) Å; b = 6.5438(11) Å; c =8.8164(7) Å with α = β = γ = 90º. The unit cell volume is 654.87 Å^3. The atomic coordinates of cations and anions of the YBO_3 unit cell are given in Table-1 and the typical unit cell of orthorhombic YBO_3 is shown in Fig. 3.

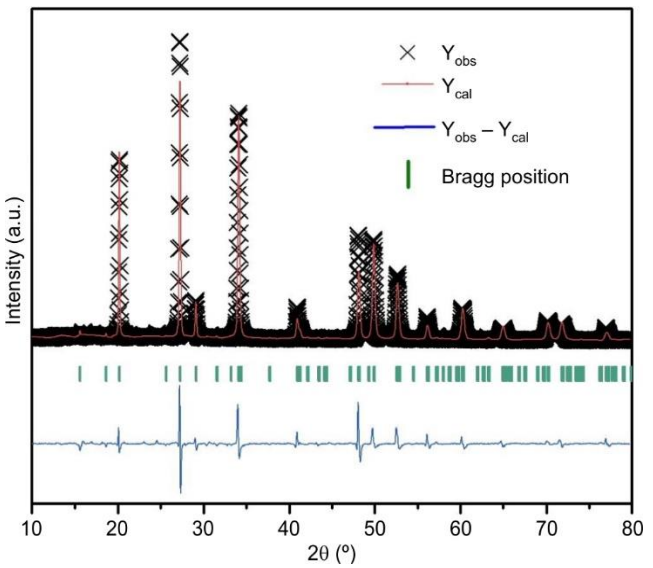

Fig. 2. Reitveld refinement results of the synthesized YBO_3 sample

TABLE-1
ATOMIC COORDINATES OF YBO_3

Atom	x	y	z	Occ.	U_{eq} (Å^2)
Y1	0.16700	0	0	1	0.0116
Y2	0	0.5	0	1	0.01612
B1	0.207(13)	0.21(3)	0.25	1	0.07876
B2	0	0.725(15)	0.25	1	0.02182
O1	0.18491	0.07729	0.25	1	0.06757
O2	0	0.36243	0.25	1	0.02136
O3	0.17669	0.32066	0.10081	1	0.00325
O4	0	0.168(9)	0.627(3)	1	0.0111

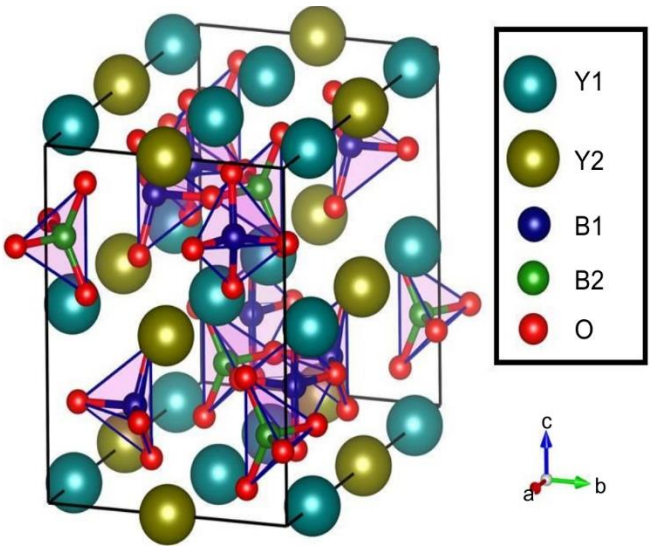

Fig. 3. Graphical representation of YBO_3 unit cell

The polyhedral structure of cations in the YBO_3 lattice can be explained as follows. In the host structure, Y^{3+} ions occupy two distinct Wyckoff positions: 4a and 8e. Each Y^{3+} ion is coordinated by eight O^{2-} ions, forming YO_8 polyhedra. At the 4a position, the Y^{3+} ion is surrounded by oxygen atoms in a distorted cubic geometry, resembling a body-centered cube. In contrast, the Y^{3+} ion at the 8e site also exhibits eight-fold coordination but adopts a geometry closer to a square antiprism. These YO_8 polyhedra share corners and edges with neighbouring YO_8 units and BO_4 tetrahedra, creating a three-dimensional network. The borate groups [BO_4] form four-fold coordinated, slightly distorted tetrahedral units. The overall crystal structure belongs to the orthorhombic *Cmcm* space group, which corresponds to the D_{2h} point group symmetry.

Understanding the coordination environment of Y^{3+} is particularly relevant for luminescence studies. Due to the similarity in ionic radii, luminescent dopants especially lanthanide ions preferentially substitute for Y^{3+} in the lattice. For instance, the Y^{3+} ion, with an ionic radius of approximately 101 pm (for CN = 8), closely matches the radii of common dopant ions such as Sm^{3+} and Ce^{3+}. These insights into coordination chemistry and site occupancy are consistent with findings reported in earlier studies and support the potential of YBO_3 as an efficient host matrix for rare-earth luminescence [16-22].

Photoluminescence excitation and emission characteristics of Sm^{3+} doped YBO_3 phosphor: The typical PL excitation spectrum of 1 mol% of Sm^{3+} doped YBO_3 phosphor are shown in Fig. 4. The excitation spectrum consists of many absorption bands such as 350, 368, 380, 408 and 423 nm. The observed absorption peaks are due to the electronic transition between the states $^6H_{5/2} \rightarrow {}^4H_{7/2}$, $^6H_{5/2} \rightarrow {}^4H_{7/2}$, $^6H_{5/2} \rightarrow {}^6P_{7/2}$, $^6H_{5/2} \rightarrow {}^6P_{7/2}$ and $^6H_{5/2} \rightarrow {}^4F_{7/2}$. These bands are attributed to the 4*f*-4*f* electronic transition of Sm^{3+} ions. Among these absorption bands, the 408 nm band is the most intense one when compared to other bands, as it has more transition probability. The representative PL emission spectra of 1 mol% of Sm^{3+} doped YBO_3 phosphor are displayed in Fig. 5. By the excitation of 408 nm, the phosphor shows emission at 572, 608 and 655 nm. The 564 nm emission has a shoulder peak at 568 nm, the 608 nm emission has shoulders at 593, 601, 612, 617, 648, 655 and 667 nm and the 649 nm emission have a shoulder at 667 nm. The observed weak shoulder peaks are due to the crystal field generated by the elements of the host lattice. The origin of shoulder peaks or splitting of emission bands due to the crystal field is often termed as Stark effect. The emission peaks 564 nm, 608 nm and 649 nm are attributed to the transitions such as $^4G_{5/2} \rightarrow {}^6H_{5/2}$, $^4G_{5/2} \rightarrow {}^6H_{7/2}$ and $^4G_{5/2} \rightarrow {}^6H_{9/2}$, respectively. The transition $^4G_{5/2} \rightarrow {}^6H_{5/2}$ is a magnetic-dipole transition and $^4G_{5/2} \rightarrow {}^6H_{9/2}$ is an electric-dipole transition. The transition $^4G_{5/2} \rightarrow {}^6H_{7/2}$ is a forced electric-dipole transition or mixed electric and magnetic-dipole transition, which is a parity-forbidden transition in the free ion state and it is partially allowed in the condensed state. In the emission spectra, the 608 nm is more intense and as a consequence the colour of the phosphor's emission is identified as red-orange [23-27]. The empirical energy level diagram of Sm^{3+} in YBO_3 is shown in Fig. 6. Further, the intensity ratio (I_{649}/I_{564}) between the electric-dipole transitions ($^4G_{5/2} \rightarrow {}^6H_{9/2}$) to the magnetic–dipole transition ($^4G_{5/2} \rightarrow {}^6H_{5/2}$) is less than one and it dictates the higher symmetry nature around the Sm^{3+} ions. It also considerably influences the orange-red emission of the Sm^{3+} ion. This nature suggests that Sm^{3+} may occupy the highly symmetric square antiprism site rather than the distorted cubic site. Also, the intensity ratio value indicates the change of co-valency between the Sm-O bond.

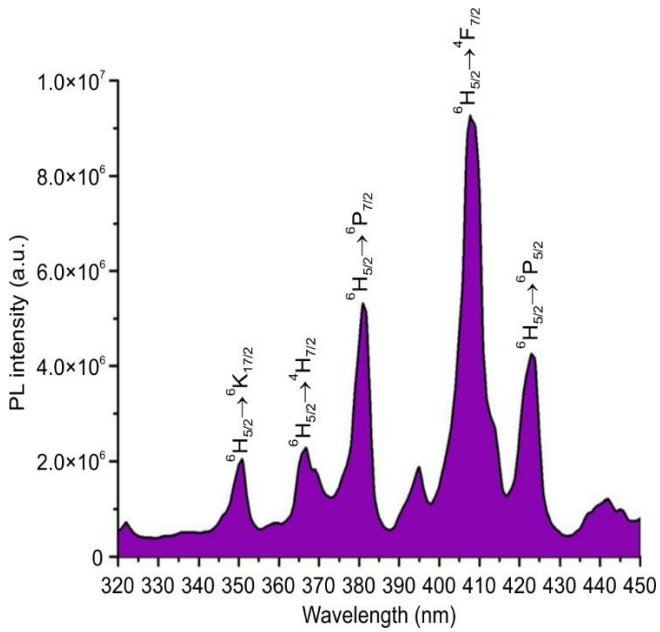

Fig. 4. PL excitation spectrum of 1 mol% of Sm^{3+} doped YBO_3 phosphor

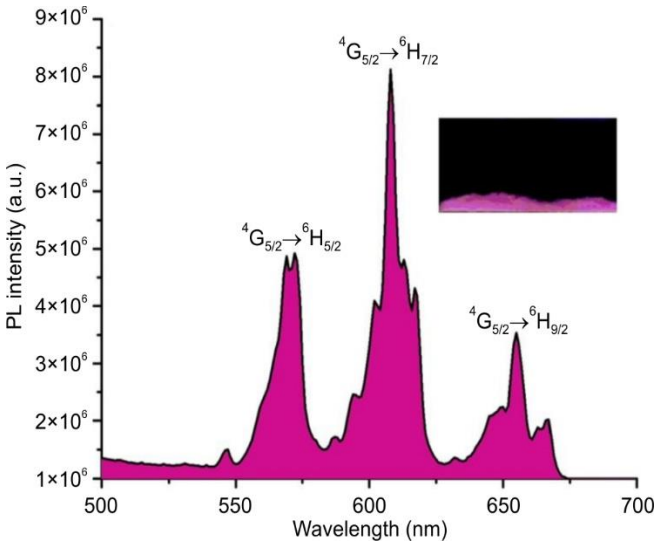

Fig. 5. PL emission spectrum of 1 mol% of Sm^{3+} doped YBO_3 phosphor (The inset shows the photograph of phosphor's orange-red emission under the UV lamp)

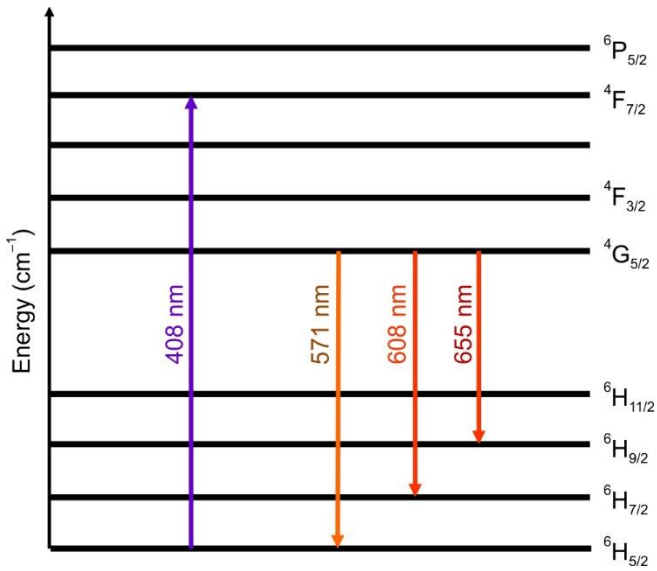

Fig. 6. Empirical energy level diagram of Sm^{3+} in YBO_3

Ce^{3+} doped YBO_3 phosphor: The typical PL excitation spectrum of 1 mol% of Ce^{3+} doped YBO_3 phosphor is shown in Fig. 7. The excitation spectrum consists of a strong and broad absorption band centered at 363 nm. The excitation at 363 nm is due to the electronic excitation from the 4*f* ground state $^2F_{5/2}$ to the 5*d*-excited state. The Ce^{3+} has the electronic configuration [Xe]5*d*4*f*^{1}. In the ground state, the configuration 4*f*^{1} is split into $^2F_{5/2}$ and $^2F_{7/2}$ states, respectively. The energy separation value between the ground states is about 1800 cm^{-1}. The ground state is split by spin-orbit interaction. The 5*d*-level of Ce^{3+} is sensitive to the crystal field of the host lattice and it varies with the field of the surrounding. By the excitation of 363 nm light, the phosphor gives emission at 415 nm in the violet-blue region with the shoulder peak at 385 nm (Fig. 8).

The observed emission is attributed to the electronic de-excitation or relaxation from the 5*d*-excited state to the ground 4*f* ground states $^2F_{5/2}$ and $^2F_{7/2}$, respectively. The emission

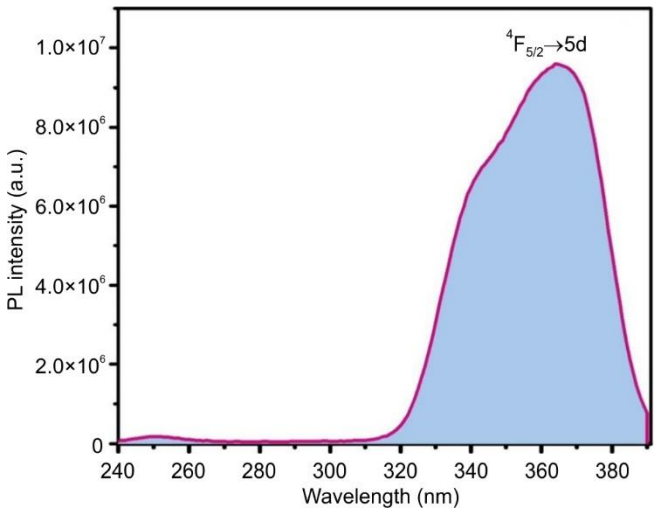

Fig. 7. PL excitation spectrum of 1 mol% of Ce^{3+} doped YBO_3 phosphor

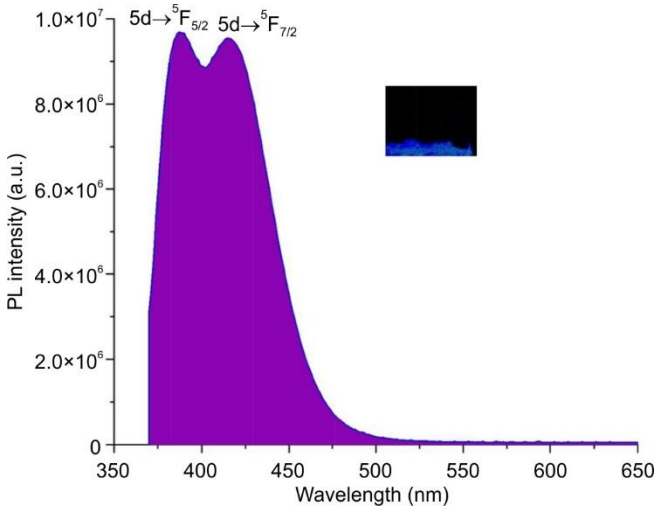

Fig. 8. PL emission spectrum of 1 mol% of Ce^{3+} doped YBO_3 phosphor (Inset shows the photograph of phosphor's violet-blue emission under the UV lamp)

peak at 415 nm is ascribed to the electronic transition 5d → $^2F_{7/2}$ and the emission at 385 nm owing to 5d → $^2F_{5/2}$ state [28,29]. The empirical energy level diagram of Ce^{3+} in YBO_3 phosphor is illustrated in Fig. 9.

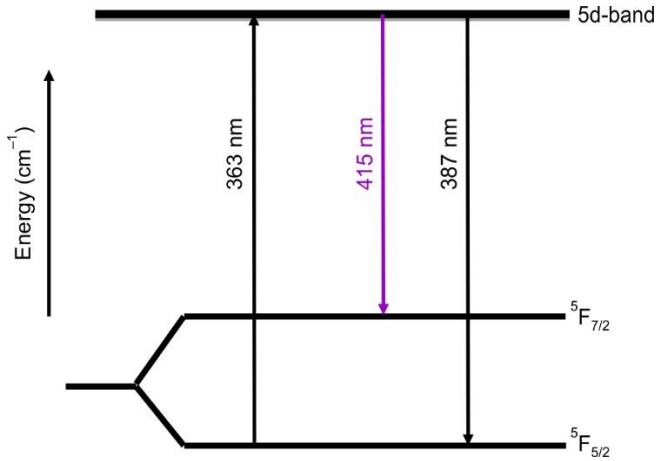

Fig. 9. Empirical energy level diagram of Ce^{3+} doped YBO_3 phosphor

Sm^{3+} and Ce^{3+} concentration effects: The change of PL intensity as a function of Sm^{3+} and Ce^{3+} concentration is depicted in Fig. 10. Samarium concentration is varied from 1 mol% to 5 mol%. The PL intensity increased up to 3 mol% and afterwards the intensity decreased. Similarly, 4 mol% of Ce^{3+} concentration gives optimal PL intensity compared to other concentrations. It explores that the resonant energy transfer takes place among the similar or identical luminescent centres when increasing the samarium and cerium concentration beyond 3 mol% and 4 mol%, respectively. The excitation energy is dissipated as non-radiative energy from one lanthanide ion (Sm^{3+}/Ce^{3+}) to another lanthanide ion (Sm^{3+}/Ce^{3+}). This effect may be due to the exchange interaction, radiation reabsorption or multipole-multipole interaction [30].

CIE chromaticity: The CIE colour chromaticity values of the phosphor were estimated using the PL emission data by using the software CIE1931xy.V.1.6.0.2a. The Sm^{3+} doped YBO_3 has the (x, y) coordinates values (x = 0.4320, y = 0.3897). The value indicates the orange-red emission of the Sm^{3+} doped phosphor. The Ce^{3+}-doped YBO_3 phosphor exhibited CIE chromaticity coordinates of (x = 0.1667, y = 0.0280), which correspond to a deep violet-blue emission. The chromaticity behaviour of both phosphors is shown in Fig. 11.

Conclusion

Yttrium borate (YBO_3) has been synthesized through a simple solid-state reaction technique at 1000 ºC. The synthesized was confirmed to crystallize in an orthorhombic crystal structure with free impurity phases. Lattice parameters of

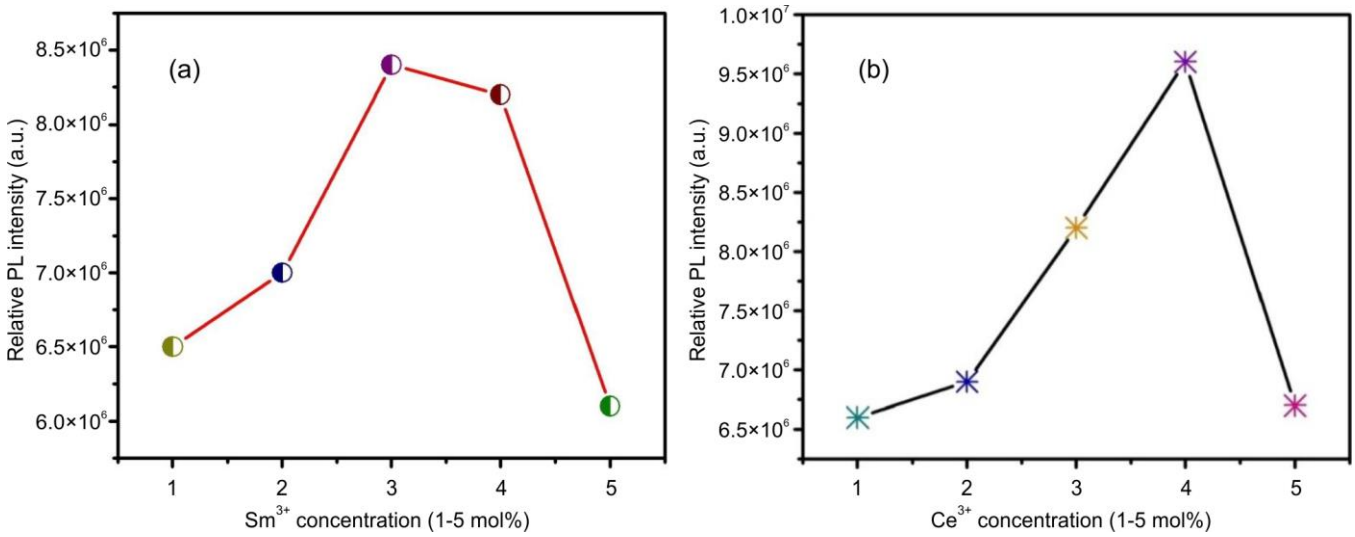

Fig. 10. Variation of PL intensity as a function of (a) Sm^{3+} and (b) Ce^{3+} concentration

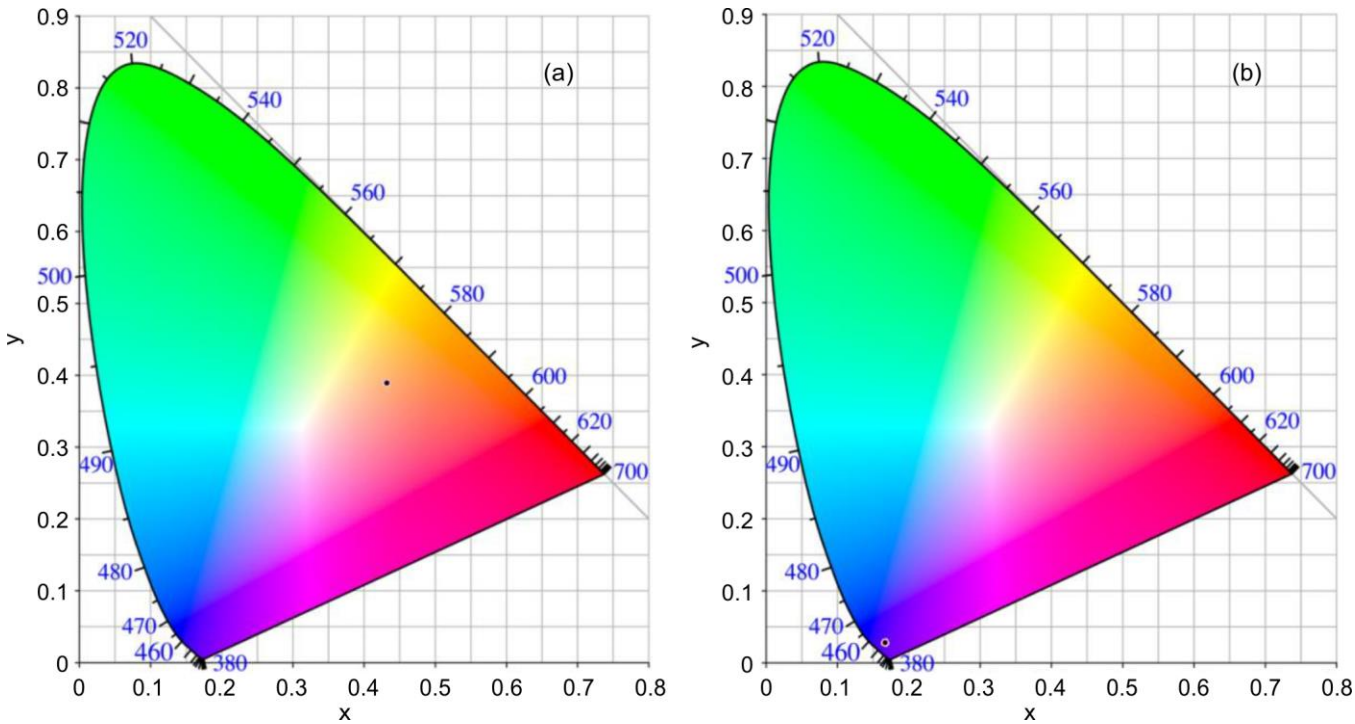

Fig. 11. CIE colour chromaticity plots of (a) YBO_3:Sm^{3+} and (b) YBO_3:Ce^{3+}

synthesized YBO_3 were also calculated and reported. Photoluminescence properties of samarium (Sm^{3+}) and cerium (Ce^{3+}) doped YBO_3 phosphors were analyzed. By the excitation of 408 nm, Sm^{3+} doped YBO_3 phosphor gives emission at 608 nm in the red region. The highest PL intensity was obtained at 3 mol% of Sm^{3+}. By the excitation of 358 nm, the Ce^{3+} doped YBO_3 phosphor gives emission at 418 nm in the violet-blue region. The highest PL intensity was obtained at 4 mol% of Ce^{3+}. Finally, it is concluded that based on the excitation and emission profile, this phosphor may find application as a red and blue emitter in phosphor-converted light emitting diodes lighting systems and counterfeit currencies.

CONFLICT OF INTEREST

The authors declare that there is no conflict of interests regarding the publication of this article.

REFERENCES

1. Y. Xiao, Y. Xu, H. Chen, Y. Ding, M. Luo, Y. Han, C. Ma and T. Zheng, *Mater. Lett.*, **360**, 135975 (2024); https://doi.org/10.1016/j.matlet.2024.135975.
2. A. Jain, P. Seth and S. Aggarwal, *Appl. Radiat. Isot.*, **206**, 111222 (2024); https://doi.org/10.1016/j.apradiso.2024.111222
3. J. Kong, H. Su, C. Li, S. Cheng, Y. Wang, Y. Ran, Y. Li, Y. Shang, S. Xie and R. Yu, *Ceram. Int.*, **49**, 39329 (2023); https://doi.org/10.1016/j.ceramint.2023.09.278
4. M. Gao, B. Cao, Z. Liao, L. Qiu, Y. He and B. Dong, *Mater. Res. Bull.*, **172**, 112667 (2024); https://doi.org/10.1016/j.materresbull.2023.112667
5. L. Reddy, *J. Fluoresc.*, **35**, 1205 (2024); https://doi.org/10.1007/s10895-023-03561-0
6. B. Fuchs, F. Schröder, G. Heymann, R. Siegel, J. Senker, T. Jüstel and H. Huppertz, *Z. Anorg. Allg. Chem.*, **647**, 2035 (2021); https://doi.org/10.1002/zaac.202100229
7. S.M. Rafiaei and A. Bahrami, *J. Nanostruct. Chem.*, **7**, 367 (2017); https://doi.org/10.1007/s40097-017-0246-1
8. Z. Yu, Y. Yang and J. Sun, *Nanomaterials*, **13**, 1013 (2023); https://doi.org/10.3390/nano13061013
9. L.T.T. My, N.L. Thai, T.M. Bui, H.-Y. Lee and N.D.Q. Anh, *Mater. Sci. Pol.*, **40**, 105 (2022); https://doi.org/10.2478/msp-2022-0050
10. S. Kang, Z. Yu, Q. Tian, M. Tai, J. Wang, D. Jin and L. Wang, *Electron. Mater. Lett.*, **18**, 540 (2022); https://doi.org/10.1007/s13391-022-00367-3
11. T. Malyi, V. Tsiumra, V. Vistovskyy, N. Mitina, H. Stryhanyuk, N. Musat, A. Kondyr, A. Zaichenko and A. Voloshinovskii, *Opt. Mater.*, **124**, 112008 (2022); https://doi.org/10.1016/j.optmat.2022.112008
12. P. Gupta, M. Sahni and S. Chauhan, *Optik*, **240**, 166810 (2021); https://doi.org/10.1016/j.ijleo.2021.166810
13. Q. Zhu, Z. Fan, S. Li and J. Li, *J. Asian Ceram. Soc.*, **8**, 542 (2020); https://doi.org/10.1080/21870764.2020.1761084
14. R.G. Nair, S. Nigam, V. Sudarsan and R.K. Vatsa, *AIP Conf. Proc.*, **2115**, 030618 (2019); https://doi.org/10.1063/1.5113457
15. S.J. Dhoble, B. Deva Prasad Raju and V. Singh, Phosphors Synthesis and Applications, Jenny Stanford Publishing (2018)
16. E.M. Levin, R.S. Roth and J.B. Martin, *Am. Mineral.*, **46**, 1031 (1961); https://doi.org/10/1030/4253522/am
17. G. Chadeyron, M. El-Ghozzi, R. Mahiou, A. Arbus and J.C. Cousseins, *J. Solid State Chem.*, **128**, 261 (1997); https://doi.org/10.1006/jssc.1996.7207
18. A. Szczeszak, S. Lis and V. Nagirnyi, *J. Rare Earths*, **29**, 1142 (2011); https://doi.org/10.1016/S1002-0721(10)60613-8
19. J.D. Chen, H. Guo, Z.Q. Li, H. Zhang and Y.X. Zhuang, *Opt. Mater.*, **32**, 998 (2010); https://doi.org/10.1016/j.optmat.2010.01.040
20. H. Hara, S. Takeshita, T. Isobe, Y. Nanai, T. Okuno, T. Sawayama and S. Niikura, *J. Alloys Compd.*, **577**, 320 (2013); https://doi.org/10.1016/j.jallcom.2013.05.203
21. A. Nohara, S. Takeshita and T. Isobe, *RSC Adv.*, **4**, 11219 (2014); https://doi.org/10.1039/c3ra47864e
22. K.A. Koparkar, N.S. Bajaj and S.K. Omanwar, *Opt. Mater.*, **39**, 74 (2015); https://doi.org/10.1016/j.optmat.2014.11.001
23. P. Li, Z. Wang, Z. Yang, Q. Guo and X. Li, *Mater. Lett.*, **63**, 751 (2009); https://doi.org/10.1016/j.matlet.2008.12.041
24. Z. Xia and D. Chen, *J. Am. Ceram. Soc.*, **93**, 1397 (2010); https://doi.org/10.1111/j.1551-2916.2009.03574.x
25. Y. Tian, Y. Liu, R. Hua, L. Na and B. Chen, *Mater. Res. Bull.*, **47**, 59 (2012); https://doi.org/10.1016/j.materresbull.2011.10.007
26. M.J. Treadaway and R.C. Powell, *Phys. Rev., B, Solid State*, **11**, 862 (1975); https://doi.org/10.1103/PhysRevB.11.862
27. R. Thomas and V.P.N. Nampoori, *Solid State Commun.*, **73**, 803 (1990); https://doi.org/10.1016/0038-1098(90)90134-W
28. W.R. Liu, C.H. Huang, C.P. Wu, Y.C. Chiu, Y.T. Yeh and T.M. Chen, *J. Mater. Chem.*, **21**, 6869 (2011); https://doi.org/10.1039/c1jm10765h
29. G. Dieke, H. Crosswhite and B. Dunn, *J. Opt. Soc. Am.*, **51**, 820 (1961); https://doi.org/10.1364/JOSA.51.000820
30. G. Blasse and B.C. Grabmaier, Luminescent Materials, Springer: Verlag Berlin Heidelberg (1994).